Parameterization of frequency domain FWI

Junxiao Li, Kris Innanen, Wenyong Pan

ABSTRACT

Full-waveform inversion (FWI) aims to update the long and short wavelengths of the perturbations, in which parameterization plays an important role in multiparameter updates. For the anisotropic inversion of a transversely isotropic medium with a vertical symmetry direction (VTI), the parameterization can be chosen as five elastic constants (c_{11}, c_{13}, c_{33}, c_{44} and density) or in other forms of parameterizations. In this paper, the choose of parameterizations is briefly discussed. The gradients of four elastic constants(vertical P-wave velocity, horizontal P-wave velocity, vertical S-wave velocity and δ) are calculated. The comparison with the inversion of elastic constants demonstrates the inversion of a combination with P- and S-wave velocities and Thomson parameters reduces interparameter crosstalks. To improve the inversion and avoid influence of one parameter with higher range of value on the inversion result than the other, the hierarchical inversion strategy is also applied in this paper. A three-layer VTI model is used to illustrate the hierarchical inversion strategy. Finally, a synthetic model is inverted with a parameterization of vertical P-wave velocity, horizontal P-wave velocity, vertical S-wave velocity and δ are illustrated.

INTRODUCTION

Application of FWI to VTI media is typically limited to the acoustic approximation (Plessix and Cao, 2011; Gholami et al., 2013b). The reason of this simplification is firstly, elastic VTI modeling is generally more computationally intensive which requires more wavefield components to be computed (Chang and McMechan, 2009; Kamath and Tsvankin, 2016; Pan et al., 2016). This implies multiparameter anisotropic elastic FWI is a highly non-linear problem; and secondly, the ill-posed inverse problem leads the misfit function to many local minima, which will even increase when multiple classes of parameters are involved in the inversion. Despite these difficulties, multiparameter elastic and anisotropic FWI is still under intensive study to better reconstruct different reservoir parameters, which in turn, provides more precise characterization of oil and gas reservoirs.

One key issue for multiparameter anisotropic FWI is to choose a suitable parameterization to describe the subsurface properties while reducing interparameter trade-offs caused from these parameters. An enlightened understanding of perturbation radiation pattern is decisive to analyze the dependency of FWI on the anisotropy parameters (Wu and Aki, 1985; Virieux and Operto, 2009). Barnes et al. (2008) used the full waveform inversion in VTI media, in which, the Thomsen parameters (Thomsen, 1986)(including isotropic parameters of vertical P- and S-wave velocities, anisotropic parameters of δ and ε) are inverted. However, the anisotropic parameters can not be well restored. Gholami et al. (2013a) also pointed out that the choice of parameterization is important for anisotropic FWI. Gholami and Siahkoohi (2010) pointed out that Thomson's parameters can not be inverted simultaneously even if source-receiver stations are well distributed at all directions. Lee et al. (2010) applied a frequency FWI in VTI medium with parameterization of stiffness constants based on sensitivity analysis with respect to different parameters. In his paper, he

coupled elastic constants c_{11} and c_{33} based on Thomsen's relationship. And the steepest-descent method based on the adjoint state of the wave equations (Lailly, 1983; Tarantola, 1984; Pratt et al., 1998) are used to updated by model parameters. Alkhalifah and Plessix (2014) and Alkhalifah (2015) analyzed FWI radiation patterns in acoustic VTI media based on pseudoacoustic wave equations. He emphasized horizontal P-wave velocity effectively reduces the number of parameters for VTI FWI. Based on radiation patterns and the relation between the perturbation of parameters and perturbation in traveltime, Da Silva et al. (2016) developed a new parameterization in the scope of FWI, which contains two velocities and one Thomsen's parameter. Moradi and Innanen (2017) analyzed the scattering of seismic waves from anisotropic-viscoelastic inclusions using the Born approximation. In this paper, he separated viscoelastic VTI media into a homogeneous viscoelastic reference medium with distributed inclusions in both viscoelastic and anisotropic properties.

In this paper, according to the partial derivative of wavefields, two parameterizations are analyzed at the begining of this paper: 1) parameterization of stiffness constants and 2) parameterization of P-wave vertical and horizontal velocities, S-wave vertical velocity and Thomson parameter δ. The comparison of inversion results with the two parameterizations show obvious cross-talks can be observed in inverted stiffness constants, and the shape and value of anomaly c_{13} are distorted. On the other hand, no obvious crosstalks are present in the inverted parameters using the other parameterization.

To improve the inversion and avoid influence of one parameter with higher range of value on the inversion result than the other, the hierarchical inversion strategy is also applied. Finally, a layered synthetic VTI model is inverted with the new parameterization.

PARAMETERIZATION

Simultaneously inverting multiple parameters suffers from interparameter tradeoffs, which increases the nonlinearity of the inverse problems((Tarantola, 1986; Alkhalifah and Plessix, 2014; Innanen, 2014).). A proper parameterization can provide with interpretable high-resolution results for FWI in VTI medium, where, multiparameters are to be inverted. On the other hand, an improper choice of parameterization can lead to local minimum. Most of the parameter resolution study is based on analytic solutions of Frechet derivative wavefields (scattering" or radiation" patterns)((Tarantola, 1986; Gholami et al., 2013b; Alkhalifah and Plessix, 2014; Moradi and Innanen, 2015)). According to Tarantola (1986), a high-resolution parameterization should have scattering patterns as different as possible . Alkhalifah and Plessix (2014) emphasized horizontal P-wave velocity effectively reduces the number of parameters for VTI FWI. In this section, we will analyze the parameterization based on the sensitivity of the partial derivative wavefields towards the pertrubations of two parameterizations (Parameterization 1: stiffness constants and parameterization 2: vertical P-wave velocity (v_{P0}), horizontal P-wave velocity (v_{h0}), vertical S-wave velocity (v_{S0}) and δ).

Wave propagation in an elastic medium is governed by:

$$\begin{aligned}\rho\partial_t^2 u_j - \sigma_{ij,j} &= f_j \\ \sigma_{ij} - c_{ijkl}\varepsilon_{kl} &= T_{ij} \\ \varepsilon_{kl} &= \tfrac{1}{2}(u_{k,l} + u_{l,k})\end{aligned} \quad . \tag{1}$$

where $i, j = 1, 2, 3$, ρ is the density, u_i is the displacement vector and σ_{ij} is stress tensor, and where $\sigma_{ij,j}$ represent spatial derivatives of the stress tensor. The comma between subscripts is used for spatial derivatives. The summation convention for repeated subscripts is assumed. And c_{ijkl} are the elastic stiffness coefficients, ε_{kl} denotes the strain tensor.

In the case of a transverse isotopic medium, the second-order wave equation system in frequency domain can be written as

$$\begin{aligned}-\rho\omega^2 u_x &= \tfrac{\partial\sigma_{11}}{\partial x} + \tfrac{\partial\sigma_{12}}{\partial y} + \tfrac{\partial\sigma_{13}}{\partial z} + f_x \\ -\rho\omega^2 u_y &= \tfrac{\partial\sigma_{21}}{\partial x} + \tfrac{\partial\sigma_{22}}{\partial y} + \tfrac{\partial\sigma_{23}}{\partial z} + f_y \\ -\rho\omega^2 u_z &= \tfrac{\partial\sigma_{31}}{\partial x} + \tfrac{\partial\sigma_{32}}{\partial y} + \tfrac{\partial\sigma_{33}}{\partial z} + f_z\end{aligned} \quad . \tag{2}$$

For formations with a vertical symmetry axis (VTI), the elastic stiffness tensor is

$$c_{VTI} = \begin{bmatrix} c_{11} & c_{11}-2c_{66} & c_{13} & 0 & 0 & 0 \\ c_{11}-2c_{66} & c_{11} & c_{13} & 0 & 0 & 0 \\ c_{13} & c_{13} & c_{33} & 0 & 0 & 0 \\ 0 & 0 & 0 & c_{44} & 0 & 0 \\ 0 & 0 & 0 & 0 & c_{44} & 0 \\ 0 & 0 & 0 & 0 & 0 & c_{66} \end{bmatrix}, \tag{3}$$

And the 2D elastic stiffness tensor is reduced to

$$c_{VTI} = \begin{bmatrix} c_{11} & c_{13} & 0 \\ c_{13} & c_{33} & 0 \\ 0 & 0 & c_{44} \end{bmatrix}. \tag{4}$$

The 2D elastic wave equations for VTI media can be written as

$$\begin{aligned}-\rho\omega^2\tilde{u}_x &= \tfrac{\partial}{\partial x}\left(c_{11}\tfrac{\partial u_x}{\partial x} + c_{13}\tfrac{\partial u_z}{\partial z}\right) + \tfrac{\partial}{\partial z}\left(c_{44}\left(\tfrac{\partial u_x}{\partial z} + \tfrac{\partial u_z}{\partial x}\right)\right) + \tilde{f}_x(\omega) \\ -\rho\omega^2\tilde{u}_z &= \tfrac{\partial}{\partial z}\left(c_{13}\tfrac{\partial u_x}{\partial x} + c_{33}\tfrac{\partial u_z}{\partial z}\right) + \tfrac{\partial}{\partial x}\left(c_{44}\left(\tfrac{\partial u_x}{\partial z} + \tfrac{\partial u_z}{\partial x}\right)\right) + \tilde{f}_z(\omega).\end{aligned} \tag{5}$$

Employing the finite-element method, the above equations can be written as

$$\mathbf{W}\tilde{\mathbf{u}} = \tilde{\mathbf{f}}. \tag{6}$$

Rewrite the above equations into the matrix formalism (Pratt and Worthington, 1988), we have

$$\begin{bmatrix} W_{xx}(\mathbf{x},\omega) & W_{xz}(\mathbf{x},\omega) \\ W_{zx}(\mathbf{x},\omega) & W_{zz}(\mathbf{x},\omega) \end{bmatrix} \begin{bmatrix} \tilde{u}_x(\mathbf{x},\omega) \\ \tilde{u}_z(\mathbf{x},\omega) \end{bmatrix} = \begin{bmatrix} \tilde{f}_x(\mathbf{x},\omega) \\ \tilde{f}_z(\mathbf{x},\omega) \end{bmatrix}, \tag{7}$$

where, $\begin{bmatrix} \tilde{f}_x(\mathbf{x},\omega) & \tilde{f}_z(\mathbf{x},\omega) \end{bmatrix}^T$ is the source vector $\tilde{f}$, and the wave operator $W(\mathbf{x},\omega)$ is defined as

$$W(\mathbf{x},\omega) = \begin{bmatrix} W_{xx}(\mathbf{x},\omega) & W_{xz}(\mathbf{x},\omega) \\ W_{zx}(\mathbf{x},\omega) & W_{zz}(\mathbf{x},\omega) \end{bmatrix}. \tag{8}$$

In VTI media, $W(\mathbf{x},\omega)$ can be written as

$$\begin{aligned} W_{xx}(\mathbf{x},\omega) &= -\rho(\mathbf{x})\omega^2 - \tfrac{\partial}{\partial x} c_{11} \tfrac{\partial}{\partial x} - \tfrac{\partial}{\partial z} c_{44} \tfrac{\partial}{\partial z} \\ W_{xz}(\mathbf{x},\omega) &= -\tfrac{\partial}{\partial x} c_{13} \tfrac{\partial}{\partial z} - \tfrac{\partial}{\partial z} c_{44} \tfrac{\partial}{\partial x} \\ W_{zx}(\mathbf{x},\omega) &= -\tfrac{\partial}{\partial z} c_{13} \tfrac{\partial}{\partial x} - \tfrac{\partial}{\partial x} c_{44} \tfrac{\partial}{\partial z} \\ W_{zz}(\mathbf{x},\omega) &= -\rho(\mathbf{x})\omega^2 - \tfrac{\partial}{\partial z} c_{33} \tfrac{\partial}{\partial z} - \tfrac{\partial}{\partial x} c_{44} \tfrac{\partial}{\partial x} \end{aligned} . \tag{9}$$

Parameterisation with stiffness constants

Frequency-domain finite-difference methods solve the matrix equation (6). By taking the partial derivative of both sides of equation (6) with respect to the kth model parameter m_k, we obtain

$$\frac{\partial \tilde{\mathbf{u}}}{\partial m_k} = \mathbf{W}^{-1} \tilde{\mathbf{f}}^{(k)}. \tag{10}$$

in which, $\tilde{\mathbf{f}}^{(k)}$ is the kth virtual source term. Based on the above equations, the partial derivative wavefields of the kth model parameter can be obtained by propagating the virtual source computed by perturbing the kth model parameter.

In order to compute partial derivative wavefields with respect to the stiffness constants, we use an semi-infinite elastic model, shown in Figure , where, the source is denoted by a yellow star, and the perturbation point is denoted as a red dot in the middle of the model, and the receivers are placed at all of the nodal points at the same depth with the source. Figure (1) also shows the residuals of the wavefields caused by perturbation of stiffness constants with an isotropic background model.

In Figures (2) to (3), we display the partial derivative of horizontal and vertical wavefields computed by perturbing stiffness constants in the center of the model. The number of each sub-figure (a)-(d) correspond to the pertrubation of c_{11}, c_{13}, c_{33} and c_{44}, respectively. The red dots are the locations of receivers. Comparing the partial derivative wavefields with each other, the horizontal components are less sensitive to the PP reflections than are the vertical components, but they are more sensitive to the PS reflections than the vertical components. In places with, small offsets, no PP reflection energy can be detected with pertrubations of different stiffness constants, except for the vertical component with a c_{33} pertrubation.

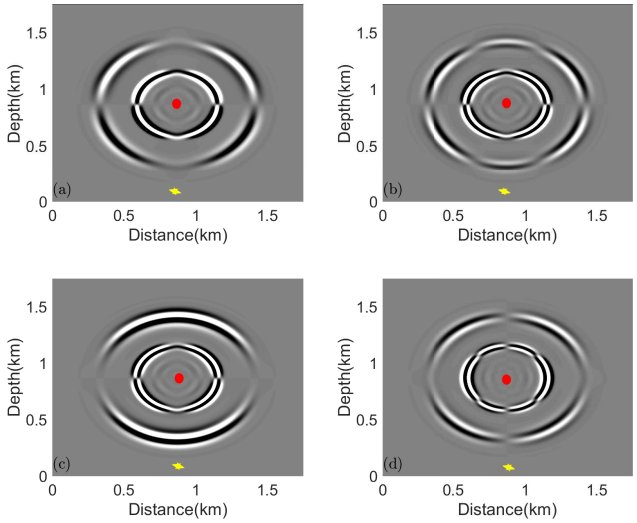

FIG. 1. Sensitivyty kernels for V_P, V_S and density in isotropic media.

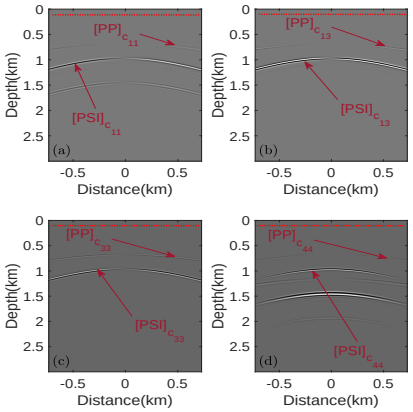

FIG. 2. Horizontal partial derivative wavefields in an isotropic background media.

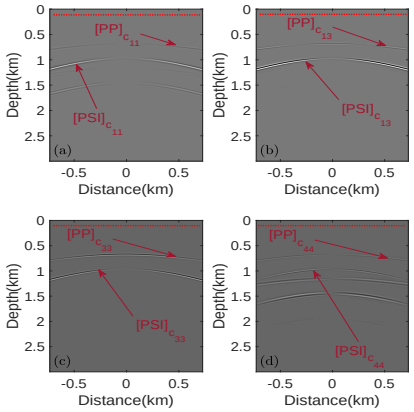

FIG. 3. Vertical partial derivative wavefields in an isotropic background media.

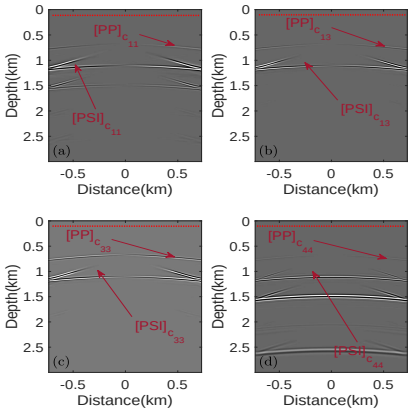

FIG. 4. The wavefields of this true model with a P-wave anomaly in the middle.

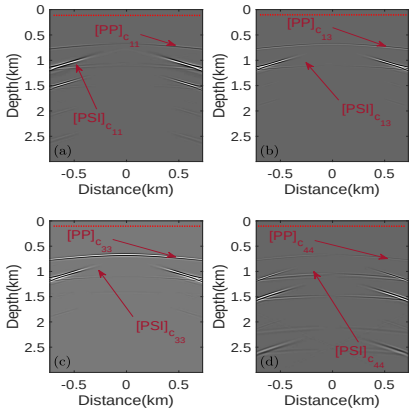

FIG. 5. The wavefields of a homogeneous initial model.

Figure (4) and (5) are horizontal and vertical wavefields computed with an anisotropic background media. The PS reflections are more distinctive in horizontal components than in vertical components. For the PP reflections, energy in small offset locations is still hard to be noticed except in vertical component with a pertrubation of c_{33}.

Parameterisation with Vertical, horizental P-wave velocity, vertical S-wave velocity and δ

The stiffness tensor can be used as quantification of scattering patterns in VTI media. Thomsen (1986) originally defined three parameters to characterize weakly anisotropic media (HTI or VTI). The stiffness tensor can thus be transformed into Thomsen parameters. In VTI media, the stiffness tensor components can be defined as

$$\begin{aligned} c_{11} &= c_{22} = \rho\,(1+2\varepsilon)\,V_{P0}^2 \\ c_{33} &= \rho V_{P0}^2 \\ c_{44} &= c_{55} = \rho V_{S0}^2 \\ c_{12} &= \rho V_{P0}^2\,[1+2\varepsilon-2(1-f)(1+2\gamma)] \\ c_{13} &= c_{23} = \rho V_{P0}^2\sqrt{f(f+2\delta)} - \rho V_{S0}^2 \end{aligned} \quad . \tag{11}$$

in which, $f = 1 - V_{S0}^2/V_{P0}^2$.

Therefore, we can compute partial derivative wavefields with respect to the new parameterization(v_{h0}, v_{P0}, v_{S0} and δ). Figure (6) shows the residuals of the wavefields caused by perturbation of new parameterization with an isotropic background model.

In Figures (7) to (8), we display the partial derivative of horizontal and vertical wavefields computed by perturbing new parameterisation in the center of the model. The number

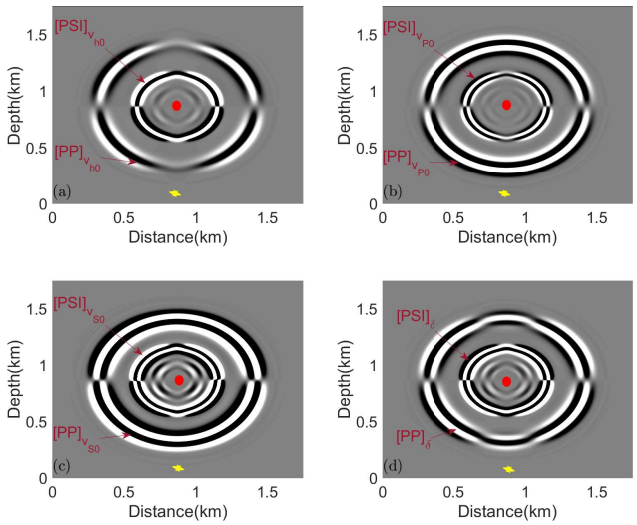

FIG. 6. Sensitivyty kernels for V_P, V_S and density in isotropic media.

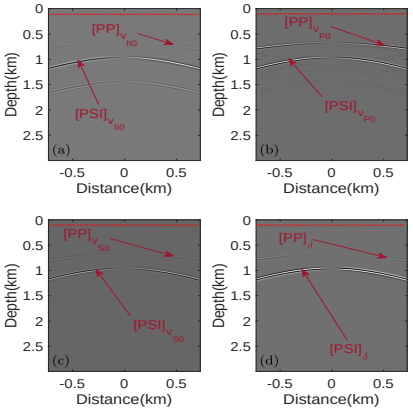

FIG. 7. The wavefields of this true model with a P-wave anomaly in the middle.

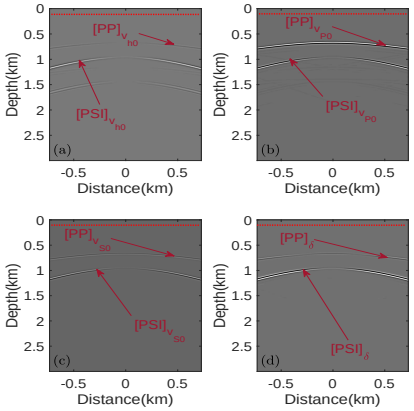

FIG. 8. The wavefields of a homogeneous initial model.

of each sub-figure (a)-(d) correspond to the pertrubation of v_{h0}, v_{P0}, v_{S0} and δ, respectively. The sensitivity to both the PP and PS reflections for pertrubations with different parameters are more dinstinctive compared with the parameterisation of stiffness constants in Figure (1).

We then display the partial derivative wavefields computed by perturbing new parameterisation in the center of the model with an anisotropic background media, shown in Figure (9) and (10), which are the horizontal and vertical components, respectively.

Comparison with two different parameterizations

In this section, a synthetic example is presented and inverted where both the above parameterizations are carried out, respectively. The density is fixed throughout the models

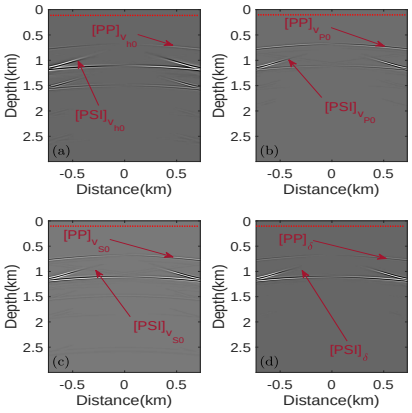

FIG. 9. The wavefields of this true model with a P-wave anomaly in the middle.

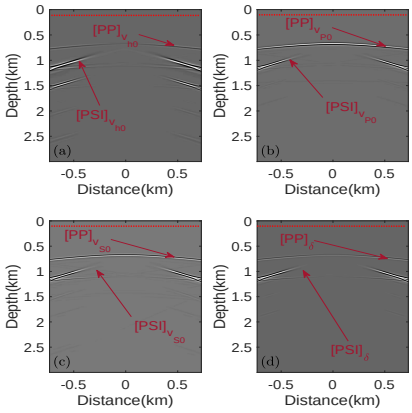

FIG. 10. The wavefields of a homogeneous initial model.

used in this paper.

The synthetic example used in this section is chosen in such a way that an anomaly of each parameter of the parameterization is present at different locations, shown in Figure (11). One of the issues when performing multiparameter inversion is that the parameters have different dynamic ranges. An appropriate scaling of the parameters can effectively improve the conditioning of the inversion(Stopin et al. (2014).Multiparameter waveform inversion of a large wide-azimuth low-frequency land data set in Oman). Instead of using an appropriate scaling, a frequency selection inversion strategy is used instead, in which some low-frequency-sensitive parameters are first updated while keeping the others unchanged. A detailed description will be discussed in the next section. In this example, the initial model is a background homogeneous VTI medium, where no anomalies are present in each parameter. The low-frequency-sensitive parameter c_{44} is first updated and the other three parameters are then updated using a prior-updated c_{44}. We sequentially perform the waveform inversion over four frequency stages: $1:0.5:5, 2:1:8, 3:2:15, 5:3:20Hz$.

In Figure (12), the value of the inverted anomaly c_{44} in Figure (12)(d) approaches the true value in Figure (11)(d). But crosstalks from the other anomalies are distinctively observed. The inverted c_{11} in Figure (12)(a) and c_{33} in Figure (12)(c) suffer less yet noticeable crosstalks than the inverted c_{44}. The shape of the inverted anomaly c_{13} is distorted and the value is relatively low compared with the true model in Figure (11)(b).

Next, we perform the multiparameter inversion using parameterization with v_{h0}, v_{P0}, v_{S0} and δ. The synthetic model shown in Figure (13) is transformed from the stiffness constant anomaly model in Figure (11). Therefore, three anomalies are present for ture $delta$ in Figure (13)(d). The low-frequency-sensitive parameter v_{S0} is also first updated while keeping the others unchanged. The initial model is a background homogeneous VTI medium, where no anomalies are present in each parameter. We sequentially perform the waveform inversion over four frequency stages: $1:0.5:5, 2:1:8, 3:2:15, 5:3:20Hz$.

In Figure (14), the value of the inverted anomaly v_{S0} in Figure (14)(b) approaches the

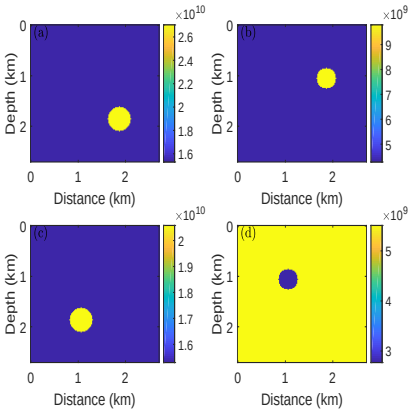

FIG. 11. True model with anomalies present in different parameters for the first parameterization.

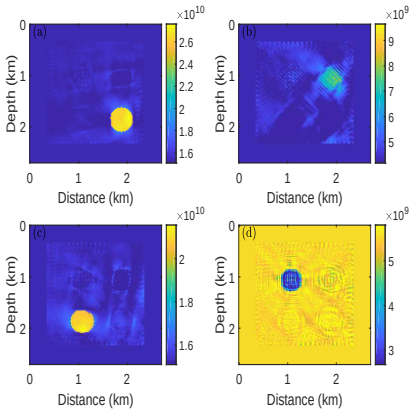

FIG. 12. FWI inverted stiffness constant model. The shape of the inverted anomaly c_{13} is distorted and the value is relatively low compared with the true model. Crosstalks are observed in the other inverted anomalies.

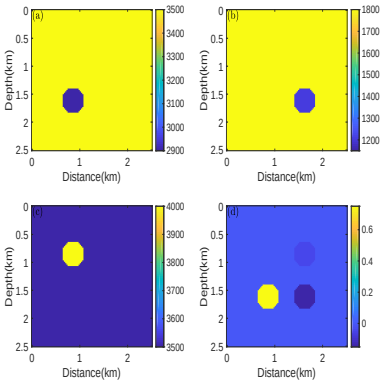

FIG. 13. True model with anomalies present in different parameters for the second parameterization.

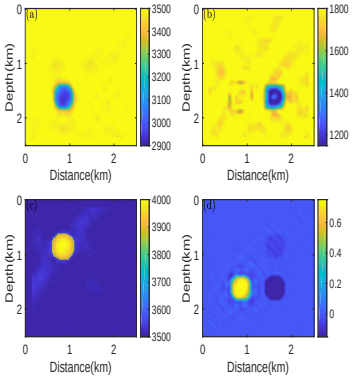

FIG. 14. FWI inverted velocity and δ model.

true value in Figure (13)(b) yet with some crosstalks from anomaly v_{h0} in Figure (13)(a). Almost no crosstalks are observed in the inverted v_{h0}, v_{P0} and δ in Figure (14)(a),(c) and (d).

THE HIERARCHICAL INVERSION STRATEGY

One of the issues of multicomponent is the fact that the parameters have different ranges. To improve the inversion and avoid influence of one parameter with higher range of value on the inversion result than the other, the hierarchical inversion strategy, as Gholami et al. (2010) demonstrated, which separates the coupled parameters across the inversion stages is thus applied in this paper.

We reduce the number of parameters at every inversion stage by applying the hierarchical inversion strategy. Therefore, some parameters are first optimized and then they are used in the next stage of the inversion.

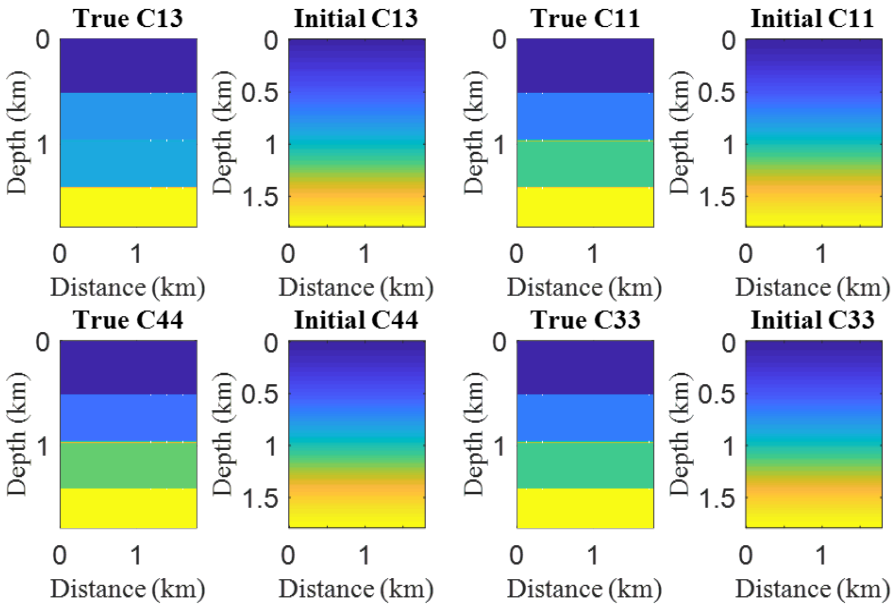

FIG. 15. True and initial three-layer VTI models.

We apply this hierarchical inversion strategy to a three-layere VTI model, shown in Figure (15), where, the true and initial models for each parameter are illustrated. The receivers are located at the surface and the sources are excited with an even spacing of 20 m at the surface. The frequency-selection strategy that sequentially performs the waveform inversion over three frequency stages(1-5 Hz, 3-8 Hz and 5-15 Hz) is applied. An interval of 0.5 Hz for each frequency stage is used. During the hierarchical inversion procedure, the parameter c_{44} is first updated while keeping the other three parameters unchanged, shown in Figure (16).

Because the partial derivative wavefield for c_{11} is similar to c_{33}, they are updated simultaneously in the next stage after an updated c_{44} is obtained, which is shown in Figure (17).

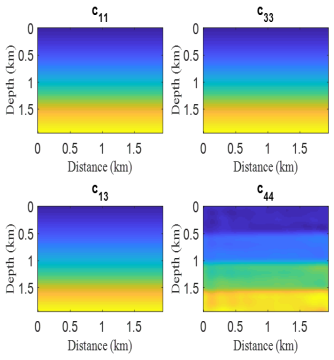

FIG. 16. Inverted c_{44} while keeping the other three parameters unchanged.

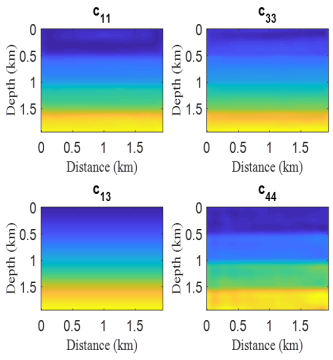

FIG. 17. Inverted c_{11} and c_{33} after c_{44} is updated.

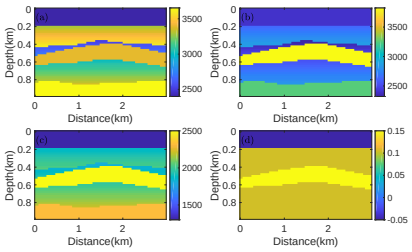

FIG. 18. True layered VTI model with perturbations of different parameters. (a) True v_{h0}; (b)True v_{P0};(c)True v_{S0}; (d)True δ .

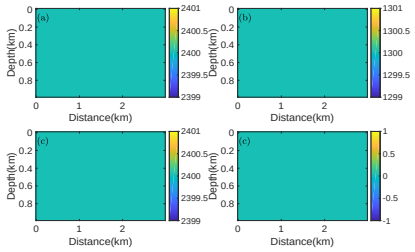

FIG. 19. Initial layered VTI model. (a) Initial v_{h0}; (b)Initial v_{P0};(c)Initial v_{S0}; (d)Initial δ.

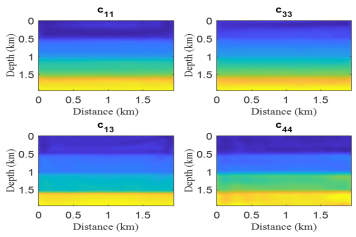

FIG. 20. True layered VTI model with perturbations of different parameters. (a) True v_{h0}; (b)True v_{P0};(c)True v_{S0}; (d)True δ .

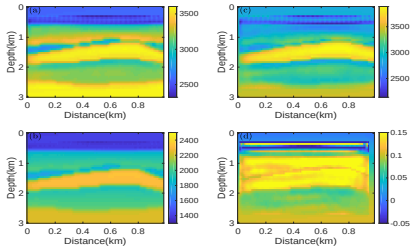

FIG. 21. Initial layered VTI model. (a) Initial v_{h0}; (b)Initial v_{P0};(c)Initial v_{S0}; (d)Initial δ.

The next stage, the last parameter c_{13} is thus updated after the other three parameters are inverted, which is shown in Figure (20). The inversion results generated by this strategy are highly compatible with the true models.

EXAMPLES

In this section, a layered VTI model with perturbations of different parameters is used to test the multiparameter inversion with the second parameterisation. The true and initial model are shown in Figure (18) ((a) True v_{h0}; (b)True v_{P0};(c)True v_{S0}; (d)True δ) and Figure (19) (Initial layered VTI model. (a) Initial v_{h0}; (b)Initial v_{P0};(c)Initial v_{S0}; (d)Initial δ).

To improve the inversion and avoid influence of one parameter with higher range of value on the inversion result than the other, the hierarchical inversion strategy is then used. We follow a similar strategy, in which the v_{S0} is first updated while keeping the other three parameters unchanged; and the parameters v_{h0} and v_{P0} are then updated; finally, the parameter δ is updated in the third stage. The inversion results are shown in Figure (21)

CONCLUSIONS

A proper parameterization may result in interpretable high-resolution results for FWI in VTI medium, where, multiparameters are to be inverted. According to the partial derivative of wavefields, two parameterizations are analyzed at the begining of this paper: 1) parameterization of stiffness constants and 2) parameterization of P-wave vertical and horizontal velocities, S-wave vertical velocity and Thomson parameter δ.

The comparison of inversion results with the two parameterizations show obvious crosstalks can be observed in inverted stiffness constants, and the shape and value of anomaly c_{13} are distorted. On the other hand, no obvious crosstalks are present in the inverted parameters using the other parameterization.

To improve the inversion and avoid influence of one parameter with higher range of value on the inversion result than the other, the hierarchical inversion strategy is also applied in this paper. A three-layer VTI model is used to illustrate the hierarchical inversion strategy, where, the stiffness constant c_{44} is first updated while keeping the other three parameters unchanged; for the second stage, the stiffness constants c_{11} and c_{33} are thus updated; the stiffness constant c_{13} is finally updated in the third stage.

Finally, a layered synthetic VTI model is inverted with the new parameterization. The lack of a comprehensive analysis of different parameterizations limits the discussion of optimized parameterizations for multiparameter VTI inversion. In this paper, only the partial derivative of the wavefields is discussed to highlight sensitivity of different perturbations towards the coverage of amplitude for PP and PS reflections, based on which, the new parameterization is used to carry out the inversion. For a future work, a comprehensive analysis of different combinations of parameterization is needed, as well as an analytical radiation patterns of corresponding combinations of parameterization.

ACKNOWLEDGMENTS

The authors thank the sponsors of CREWES for continued support. This work was funded by CREWES industrial sponsors, NSERC (Natural Science and Engineering Research Council of Canada) through the grant CRDPJ 461179-13, and by the Canada First Research Excellence Fund.

REFERENCES

Alkhalifah, T., 2015, Conditioning the full-waveform inversion gradient to welcome anisotropy: Geophysics, **80**, No. 3, R111–R122.

Alkhalifah, T., and Plessix, R.-É., 2014, A recipe for practical full-waveform inversion in anisotropic media: An analytical parameter resolution study: Geophysics, **79**, No. 3, R91–R101.

Barnes, C., Charara, M., and Tsuchiya, T., 2008, Feasibility study for an anisotropic full waveform inversion of cross-well seismic data: Geophysical Prospecting, **56**, No. 6, 897–906.

Chang, H., and McMechan, G., 2009, 3d 3-c full-wavefield elastic inversion for estimating anisotropic parameters: A feasibility study with synthetic data: Geophysics, **74**, No. 6, WCC159–WCC175.

Da Silva, N. V., Ratcliffe, A., Vinje, V., and Conroy, G., 2016, A new parameter set for anisotropic multiparameter full-waveform inversion and application to a north sea data set: Geophysics, **81**, No. 4, U25–U38.

Gholami, A., and Siahkoohi, H., 2010, Regularization of linear and non-linear geophysical ill-posed problems with joint sparsity constraints: Geophysical Journal International, **180**, No. 2, 871–882.

Gholami, Y., Brossier, R., Operto, S., Ribodetti, A., and Virieux, J., 2013a, Which parameterization is suitable for acoustic vertical transverse isotropic full waveform inversion? part 1: Sensitivity and trade-off analysis: Geophysics.

Gholami, Y., Brossier, R., Operto, S., Ribodetti, A., and Virieux, J., 2013b, Which parametrization for acoustic vti full waveform inversion? part 1: Sensitivity and trade-off analysis: Geophysics, **78**, No. 2, R81–R105.

Innanen, K. A., 2014, Seismic avo and the inverse hessian in precritical reflection full waveform inversion: Geophysical Journal International, **199**, No. 2, 717–734.

Kamath, N., and Tsvankin, I., 2016, Elastic full-waveform inversion for vti media: Methodology and sensitivity analysis: Geophysics, **81**, No. 2, C53–C68.

Lailly, P., 1983, The seismic inverse problem as a sequence of before stack migrations.

Lee, H.-Y., Koo, J. M., Min, D.-J., Kwon, B.-D., and Yoo, H. S., 2010, Frequency-domain elastic full waveform inversion for vti media: Geophysical Journal International, **183**, No. 2, 884–904.

Moradi, S., and Innanen, K. A., 2015, Scattering of homogeneous and inhomogeneous seismic waves in low-loss viscoelastic media: Geophysical Journal International, **202**, No. 3, 1722–1732.

Moradi, S., and Innanen, K. A., 2017, Born scattering and inversion sensitivities in viscoelastic transversely isotropic media: Geophysical Journal International, **211**, No. 2, 1177–1188.

Pan, W., Innanen, K. A., Margrave, G. F., Fehler, M. C., Fang, X., and Li, J., 2016, Estimation of elastic constants for hti media using gauss-newton and full-newton multiparameter full-waveform inversion: Geophysics, **81**, No. 5, R275–R291.

Plessix, R.-E., and Cao, Q., 2011, A parametrization study for surface seismic full waveform inversion in an acoustic vertical transversely isotropic medium: Geophysical Journal International, **185**, No. 1, 539–556.

Pratt, R. G., Shin, C., and Hick, G., 1998, Gauss–newton and full newton methods in frequency–space seismic waveform inversion: Geophysical Journal International, **133**, No. 2, 341–362.

Pratt, R. G., and Worthington, M., 1988, The application of diffraction tomography to cross-hole seismic data: Geophysics, **53**, No. 10, 1284–1294.

Tarantola, A., 1984, Inversion of seismic reflection data in the acoustic approximation: Geophysics, **49**, No. 8, 1259–1266.

Tarantola, A., 1986, A strategy for nonlinear elastic inversion of seismic reflection data: Geophysics, **51**, No. 10, 1893–1903.

Thomsen, L., 1986, Weak elastic anisotropy: Geophysics, **51**, No. 10, 1954–1966.

Virieux, J., and Operto, S., 2009, An overview of full-waveform inversion in exploration geophysics: Geophysics, **74**, No. 6, WCC1–WCC26.

Wu, R.-S., and Aki, K., 1985, Scattering characteristics of elastic waves by an elastic heterogeneity: Geophysics, **50**, No. 4, 582–595.